International Journal of Design Engineering

ISSN online: 1751-5882 - ISSN print: 1751-5874
https://www.inderscience.com/ijde

Contour optimisation of polygon shaft-hub connections for gearbox applications

Maximilian Schuster, Detlev Petersen, Frank Koppenhagen

DOI: 10.1504/IJDE.2022.10052166

Article History:
Received: 08 June 2022
Accepted: 31 August 2022
Published online: 20 April 2023

Contour optimisation of polygon shaft-hub connections for gearbox applications

Maximilian Schuster*

Department of Mechanical Engineering and Production Management,
Hamburg University of Applied Sciences (HAW Hamburg),
Hamburg, Germany
and
Engine Design Department,
Nord Drivesystems,
Bargteheide, Germany
Email: maximilian.schuster@aol.com
*Corresponding author

Detlev Petersen

Gear Development Department,
Nord Drivesystems,
Bargteheide, Germany
Email: dr.detlev.petersen@nord.com

Frank Koppenhagen

Department of Mechanical Engineering and Production Management,
Hamburg University of Applied Sciences (HAW Hamburg),
Hamburg, Germany
Email: frank.koppenhagen@haw-hamburg.de

Abstract: In this work, we determine the optimal geometry of complex trochoid polygon contours with respect to the stresses occurring in the shaft-hub connection. For this purpose, we carried out FEM calculations to investigate the influence of the different contour types as well as the variable parameters eccentricity and number of carriers on the level of stress occurring in the connection. With that, we derived concrete design and dimensioning guidelines for the use of polygon contours as a shaft-hub connection. Subsequently, we compared the static and dynamic load bearing capacity of a polygon connection designed according to these guidelines with a feather key connection by means of empirical tests and analytical calculations. It was shown that the H-contour is a particularly suitable solution. It showed low stress levels in the FEM calculations, and a higher static and dynamic load bearing capacity than the feather key connection in the empirical tests.

Keywords: feather key connection; polygon shaft-hub connection; finite element method; FEM; stress analysis; contour optimisation; static and dynamic load bearing capacity.

Reference to this paper should be made as follows: Schuster, M., Petersen, D. and Koppenhagen, F. (2022) 'Contour optimisation of polygon shaft-hub connections for gearbox applications', *Int. J. Design Engineering*, Vol. 11, No. 2, pp.77–102.

Biographical notes: Maximilian Schuster received his Bachelor's degree in Mechanical Engineering with a major in Engineering Design and Product Development from the Hamburg University of Applied Sciences in Hamburg, Germany, in 2019. In 2021, he received his Master's degree in Engineering Design and Product Development, also from the Hamburg University of Applied Sciences. He wrote his Master's thesis on the use of polygon shaft-hub connections for transmission applications. Since 2021, he has been working as a Design Engineer in the Engine Design Department at Nord Drivesystems in Bargteheide, Germany.

Detlev Petersen studied Precision Mechanics and Control Engineering at the Technical University of Braunschweig and received his PhD in 1989 from the Institute for Design Engineering (formerly Prof. Roth). Since 1990, he has worked for various well-known companies in the field of drive technology. In 2009, he took over the management of the Gear Development Department at Nord Drivesystems in Bargteheide, Germany. His field of activity also includes the technical supervision of dual students in the mechanical engineering department.

Frank Koppenhagen is a Professor of Engineering Design and Product Development at the Hamburg University of Applied Sciences in Hamburg, Germany and has held this position since 2009. He received his PhD in Mechanical Engineering from the Technical University of Hamburg in 2004 and worked in different capacities in passenger car development at the Mercedes-Benz Technology Center in Sindelfingen, Germany before he was appointed Professor. His research focuses on engineering design methodology and modular product architectures. He has authored and co-authored several publications in these fields. In 2012, he received the Hamburg Award for excellence in academic teaching. In 2019, he was Visiting Professor at the Center for Design Research at Stanford University in Palo Alto, CA, where he researched hybrid product development approaches based on design thinking.

1 Introduction

The drive technology is increasingly confronted with requirements for higher power densities and greater material utilisation to exploit saving potentials and meet new environmental protection requirements. Nevertheless, reliable, and low-maintenance operation must be ensured. These developments also lead to higher requirements for shaft-hub connections in modern power trains.

Polygon shaft-hub connections enable an evenly distributed transmission of torque over the circumference of the connection with a low notch effect compared to other form-fitting shaft-hub connections. Despite these significantly better mechanical properties compared to the widely used feather key connection, the industrial use of polygon shaft-hub connections has so far generally been limited to special applications. The inadequate standardisation of polygon contours has been a major obstacle to their widespread use. Until recently, there were only two standardised polygon profiles in German-speaking

countries, the P3G (DIN 32711) (DIN Deutsches Institut für Normung e.V., 2009a) and the P4C profile (DIN 32712) (DIN Deutsches Institut für Normung e.V., 2009b).

The P3G-profile is a special form of the general trochoid and is a harmonic curve that has constant thickness properties. It includes three carrier elements. On the other hand, the P4C-profile is a non-circular shaft profile that is ground over in a circular manner so that its corners are cut by a concentric circular cylinder. Therefore, it is a discontinuous profile (Frank et al., 2003). The profiles differ essentially in terms of self-centring and axial displaceability under load. In contrast to the P3G-profile, the P4C-profile is well suited for connections that must be axially displaceable under torsional load due to low normal forces, and thus also lower frictional forces. However, unlike the P3G-profile, it is not self-centring under torsional load (DIN Deutsches Institut für Normung e.V., 2009a, 2009b).

A major problem with both the P3G and P4C profiles is the lack of geometric similarity between the profiles, as shown in Figure 1. The two profiles do not have the same mathematical basis. Moreover, the P4C profile is not described by a continuous function but is composed of two combined functions. The standards mentioned define separate gradations for both profiles based on the nominal diameter d and the eccentricity e. This results in the relative eccentricity ε, which is defined according to equation (1), not being constant, as can be seen in Figure 1. Accordingly, there is no geometric similarity within the profile rows. Modern strength calculations using FEM require geometric similarity of the profiles to limit the effort required to calculate connections of different sizes by using scaling effects (Frank et al., 2003).

$$\varepsilon = \frac{e}{d} \tag{1}$$

Figure 1 Relative eccentricity ε of the P3G and P4C profile as a function of the nominal diameter (see online version for colours)

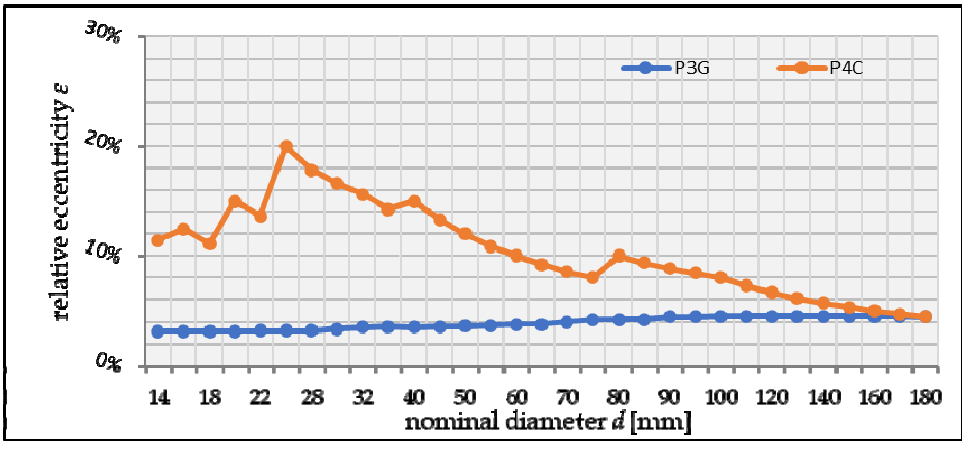

In addition, the nominal diameter d and the eccentricity e have different independent dimensional tolerances. However, since e determines the shape in the context of the standard, a change in the dimensional tolerance for e leads to a shape deviation of the polygon contour. This circumstance derives historically from the polygon grinding machines that were previously used to manufacture these profiles. However, it

contradicts today's understanding of shape and dimensional tolerances (Frank et al., 2003).

The calculation bases and dimensioning guidelines specified in the standard no longer meet the current state of the art. They are essentially based on three different calculation approaches. Said calculation approaches lead to different results and have not been validated by numerical methods (Frank and Pflanzl, 1998). Furthermore, there are no dimensioning guidelines for fatigue strength (Frank and Pflanzl, 1998).

To overcome the shortcomings of the P3G and P4C-profiles outlined above, new polygon contours that are based on complex trochoid profiles have been developed (for an overview see, Ziaei, 2007a, 2007b). The shape of these profiles is defined by the radius, the eccentricity, and number of carriers. Since these profiles are relatively new, there is still a lack of design and dimensioning guidelines for their practical use as a shaft-hub connection. This has hindered their widespread use in industry so far. The recently published DIN 3689-1 (DIN Deutsches Institut für Normung e.V., 2020) only describes the geometry of these profiles but does not include dimensioning guidelines.

The main goal of this work is to develop concrete design and dimensioning guidelines for polygon shaft-hub connections based on trochoid contours. To do so, we first analysed the influence of the different trochoid profiles and their defining parameters on the stresses occurring in the shaft-hub connection using extensive FEM calculations. Based on the results of these calculations, we derived concrete dimensioning guidelines for the selection of trochoid polygon profiles that incur minimal stresses in the shaft-hub connection. The calculations were subsequently validated by empirical tests in which we investigated the static and dynamic load bearing capacity of a polygon profile designed according to the guidelines developed. We compared the results to a standard feather key connection with the same shaft diameter and showed the differences in load bearing capacity as well as material and installation space utilisation between these two shaft-hub connections.

2 State of research

Ziaei (2003) derives an analytical calculation concept for the design of torsionally loaded non-circular profile shafts and optimises the contours of P3G and P4C profiles in terms of load bearing capacity through extensive FEM investigations. Ziaei (2007a) develops the contour geometries for new polygonal shafts based on complex cycloids and develops analytical equations to calculate the torsional stresses in the shaft and hub. In a continuing paper, Ziaei (2012) shows by means of analytical calculation that the contours based on complex trochoids are superior to comparable tooth shaft profiles according to DIN 5480 in terms of load carrying capacity under torsional load.

Großmann (2007) investigates both numerically and experimentally the influence of polygonal shafts' profile shapes on the fretting fatigue and derives approaches to enhance the fretting fatigue strength of P3G profiles and P4C profiles.

Leidich et al. (2016) compare the static limit loads of two selected polygon contours using numerical calculation. They determine the potential crack location in an H3 and an H7 profile and compare the stresses in both profiles. For stress-sensitive applications, Leidich et al. (2016) therefore recommend profiles with concave flank geometry, i.e., with low eccentricity and a small number of carriers.

Based on numerical calculations and experiments, Vetter et al. (2020) developed an analytical calculation concept for determining the fatigue strength of hypotrochoid polygon-shaft-hub connections.

DIN 3689-1 (DIN Deutsches Institut für Normung e.V., 2020) defines the geometries and dimensions of continuous hypotrochoid polygon profiles. However, it does not provide instructions for calculation and dimensioning.

The literature survey shows the lack of a systematic investigation of the optimum geometry parameters of a wide range of different trochoid polygon contours. Furthermore, no comparison has yet been made between the new trochoid polygon profiles and the still widely used feather key connections in terms of dynamic and static load bearing capacity as well as material and installation space utilisation. To close this gap, this work firstly deals with the numerical calculation and comparison of different trochoid polygon contours and secondly compares the dynamic and static load bearing capacity as well as the space utilisation of a selected polygon profile to a conventional feather key connection.

3 Mathematical foundations of trochoid polygon contours

The contours examined within this article can be derived from general cycloids and are referred to as trochoids. A trochoid is created by a defined point *P*, which is firmly connected to the rolling circle K_R. The eccentricity denotes the distance between this point *P* and the centre of the rolling circle *M*, and is shown in Figure 2. The trochoids are divided into two groups. If the circle rolls on the outside of the base circle K_B, it is called an epitrochoid. If it rolls inside, it is called a hypotrochoid (Erven and Schwägerl, 2011).

Figure 2 Creation of epi-and hypotrochoids

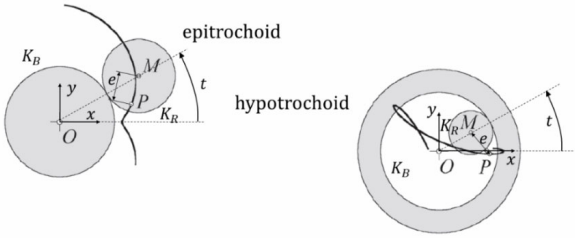

Source: Erven and Schwägerl (2011)

To create a closed contour, the radius ratio of the two circles must be rational and integer so that the contour is closed after one rotation (Erven and Schwägerl, 2011).

Taking the radius ratio into account, the epitrochoids, or short e-profiles, can be described by the parameter equations (2) and (3), where *n* describes the periodicity or corner number of the geometry, *r* the nominal radius of the profile, and *t* the parameter angle (Ziaei, 2007a):

$$x(t) = r * \cos(t) + e * \cos(n+1) * t \tag{2}$$

$$y(t) = r * \sin(t) + e * \sin(n+1) * t \tag{3}$$

Hypotrochoids, or short H-profiles, can be described by the parameter equations (4) and (5) (Ziaei, 2007a):

$$x(t) = r * \cos(t) + e * \cos[(n-1) * t] \tag{4}$$

$$y(t) = r * \sin(t) - e * \sin[(n-1) * t] \tag{5}$$

The first part of the upcoming DIN 3689 (DIN Deutsches Institut für Normung e.V., 2020) – for the new standardisation of polygon profiles – was presented to the public for review at the end of 2020 and is based on the H-profile. In it, a suggestion for the general procedure for selecting the parameters for an H-profile, based on the available installation space, can be found.

Ziaei (2007a) developed new types of complex trochoid profiles to combine the positive properties of polygon profiles with those of splined shaft profiles. All trochoids described up to this point have constant eccentricities. In this case, the periodicity is described as the first periodicity. If the eccentricity is now allowed to vary periodically, a multitude of new complex periodic profiles opens up (Ziaei, 2007a).

In theory, any number of additional eccentricities can be built in, as shown in Figure 3.

Figure 3 Creation of a complex trochoid (see online version for colours)

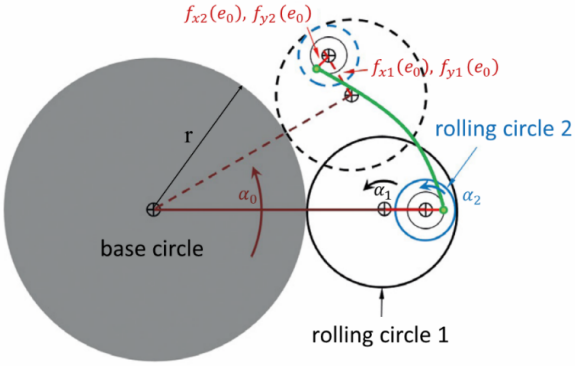

Source: Selzer and Ziaei (2016)

The parameter equation of all complex cycloids is described by the following equations (6) and (7):

$$\begin{aligned} x(t) = {} & r * \cos(\alpha_0) + f_{x1}(e_0) * \cos(\alpha_1) + f_{x1}(e_0) * \cos(\alpha_2) \\ & + f_{x3}(e_0) * \cos(\alpha_3) + f_{x4}(e_0) * \cos(\alpha_4) \end{aligned} \tag{6}$$

$$\begin{aligned} y(t) = {} & r * \sin(\alpha_0) + f_{y1}(e_0) * \sin(\alpha_1) + f_{y2}(e_0) * \sin(\alpha_2) \\ & + f_{y3}(e_0) * \sin(\alpha_3) + f_{y4}(e_0) * \sin(\alpha_4) \end{aligned} \tag{7}$$

where α_1 to α_4 are functions of the main parameter angle t. The functions f_{xn} and f_{yn} are independent of each other and describe the eccentricities, which add to the parameter equation of the trochoid. These are always dependent on the basic eccentricity e_0. Depending on which eccentricity function is used in the equations, the complex cycloids are divided into different types (Ziaei, 2007a).

One speaks of pure complex epitrochoids (E-T04) if all 4 f_{xn}-functions correspond to the f_{yn}-functions, according to condition (8). For pure complex hypotrochoids (H-T04), condition (9) must be fulfilled:

$$f_{x1} = f_{y1},\ f_{x2} = f_{y2},\ f_{x3} = f_{y3},\ f_{x4} = f_{y4} \tag{8}$$

$$f_{x1} = -f_{y1},\ f_{x2} = -f_{y2},\ f_{x3} = -f_{y3},\ f_{x4} = -f_{y4} \tag{9}$$

The main parameter angle functions used for the E-T04 profiles are described in equations (10) and in (11) for the H-T04 profiles:

$$\alpha_i = (i * n + 1) + t \tag{10}$$

$$\alpha_i = (i * n - 1) + t \tag{11}$$

Accordingly, the eccentricity function used for the E-T04 and H-T04 profiles are listed in Table 1.

Table 1 Eccentricity functions E-T04 and H-T04 profile

Eccentricity functions E-T04	*Eccentricity functions H-T04*
$f_{x1}(e_0) = f_{y1}(e_0) = e_0$	$f_{x1}(e_0) = -f_{y1}(e_0) = e_0$
$f_{x2}(e_0) = f_{y2}(e_0) = \frac{e_0}{3}$	$f_{x2}(e_0) = -f_{y2}(e_0) = \frac{e_0}{16}$
$f_{x3}(e_0) = f_{y3}(e_0) = \frac{e_0}{9}$	$f_{x3}(e_0) = -f_{y3}(e_0) = -\frac{e_0}{32}$
$f_{x4}(e_0) = f_{y4}(e_0) = \frac{e_0}{27}$	$f_{x4}(e_0) = -f_{y4}(e_0) = -\frac{e_0}{64}$

If the complex epitrochoids and hypotrochoids are combined, hybrid complex trochoids profiles (M-T04) can be generated. Here, the f_{xn}-functions correspond to the f_{yn}-functions only in terms of the number of functions. The algebraic sign can vary as desired, as shown in Table 2. It must be noted that an increase in the parameters n or e can quickly lead to contours that have undercuts and are therefore no longer interesting for technical applications due to their limited manufacturability (Ziaei, 2007a).

Table 2 Eccentricity and main parameter angle functions M-T04 profile

Eccentricity functions	*Main parameter angle functions*
$f_{x1}(e_0) = -f_{y1}(e_0) = -2 * e_0$	$\alpha_1 = (n - 1) * t$
$f_{x2}(e_0) = f_{y2}(e_0) = -e_0$	$\alpha_2 = (n + 1) * t$
$f_{x3}(e_0) = -f_{y3}(e_0) = \frac{7 * e_0}{8}$	$\alpha_3 = (2 * n - 1) * t$
$f_{x4}(e_0) = f_{y4}(e_0) = \frac{e_0}{27}$	$\alpha_4 = (2 * n + 1) * t$

The complex profiles have three main decisive advantages for technical applications compared to the conventional splined shaft profiles as well as the previous P3G and P4C polygon connections:

- Compared to the splined shaft profiles, the contours are continuous. This ensures uniform centring over the entire circumference, not just over the flanks.
- The curvature at the profile contour is precisely adjustable due to the additional built-in eccentricities. Thus, the contour can not only be adjusted precisely to the applications and loads, but also optimised for different types of production.
- The number of load bearing profile flanks can be selected as desired (Ziaei, 2007a).

Figure 4 shows an example of all the profiles described above, each with six carriers ($n = 6$).

Figure 4 Examined polygon profiles (see online version for colours)

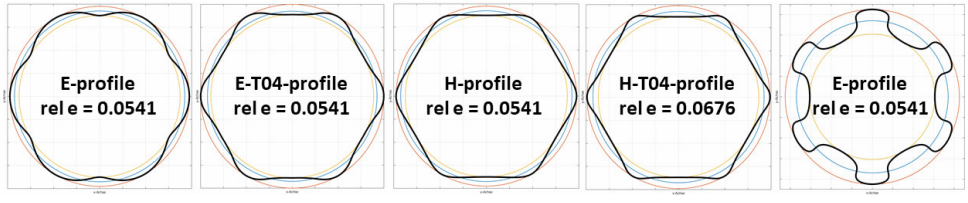

4 Methods

First, extensive FEM calculations are carried out to determine the influence of the different contour types as well as the variable parameters eccentricity and number of carriers on the level of stress occurring in the connection.

Subsequently, empirical tests are carried out to compare the most suitable polygon contour based on the FEM calculations with a feather key connection in terms of static and dynamic load bearing capacity. For the discussion of the test results, we used analytical calculations, which also show the differences between the polygon connection and the feather key connection with regard to material and installation space utilisation.

5 FEM calculations

In the first step, we compared the influence of the eccentricity parameters and the number of carriers on the equivalent von Mises stresses occurring in the profiles by using a finite element method (FEM) calculation. Based on these results, we determined the most suitable profile for the subsequent practical tests.

5.1 FEM – calculation parameters

When selecting and optimising a polygon profile, it is crucial to determine the influence of the different parameters on the notch effect of the polygon shaft-hub connection, since it directly affects the maximum stresses acting in the connection. For this purpose, different polygon profiles are calculated by using the FEM software ANSYS 19, varying the parameters of eccentricity and number of carriers. The calculated equivalent von Mises stresses can be used to illustrate the influence of the eccentricity and number of

carriers for different polygon profiles. Figure 5 shows the calculation plan of the different profiles depending on the eccentricity and number of carriers. As can be seen, the focus is placed on the H-profile. The maximum values of normal stress, shear stress, equivalent von Mises stress, frictional stress, and compressive stress in the contact area were output.

Figure 5 FEM calculation plan (see online version for colours)

		Number of carriers n				
		3	**4**	**5**	**6**	**8**
Eccentricity e	**0.1**				MT	
	0.2	H, MT	H, MT	H, MT	H, E, HT, ET, MT	H, MT
	0.3				MT	
	0.4	H, E	H, E	H, E	H, E, HT, ET, MT	H, E
	0.6	H, HT, ET	H, HT, ET	H, HT, ET	H, E, HT, ET	H, HT, ET
	0.8	H	H	H	H, E, HT, ET	H
	1.0	H	H	H	H, E, HT, ET	H

Note: E ≙ E-profile, ET ≙ E-T04-profile, H ≙ H-profile, HT ≙ H-T04-profile, MT ≙ M-T04-profile.

Tet10 elements were used in the meshing of the polygon contour. These are tetrahedral elements with quadratic approach functions, which usually achieve better results at the expense of calculation time, compared to linear approach functions.

Figure 6 ANSYS 19 automatically generated mesh of shaft and hub (see online version for colours)

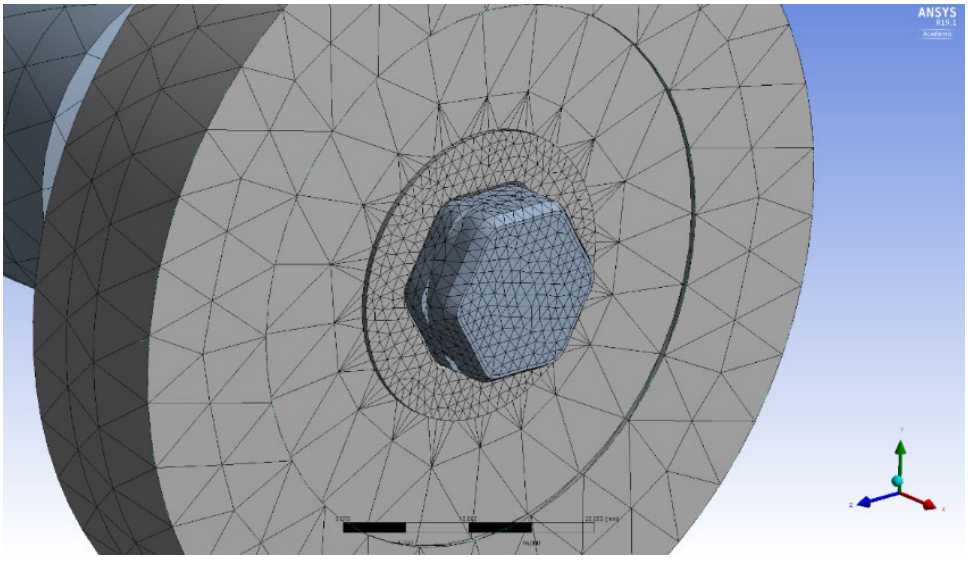

Generally, the geometry was meshed with elements with an average size of 6 mm. On the contact surfaces of the connection, the geometry was meshed with an average element size of 1 mm up to a depth of approx. 5 mm (seen Figure 6). The convergence analysis has shown that further reducing the element size does not provide more accurate results.

Using Penta15 or Hexa27 elements would allow enhanced mapping of both the symmetries of the profiles and the contour itself (Großmann, 2007; Leidich et al., 2016). However, said elements would not allow for a fully automatic meshing of the large number of different models entailing a very high manual meshing effort. Therefore, Tet10 elements were used here to limit the effort.

Figure 7 ANSYS 19 graphical examples result of the H-profile with six carriers and an eccentricity of 0.4 mm (Nord Drivesystems) (see online version for colours)

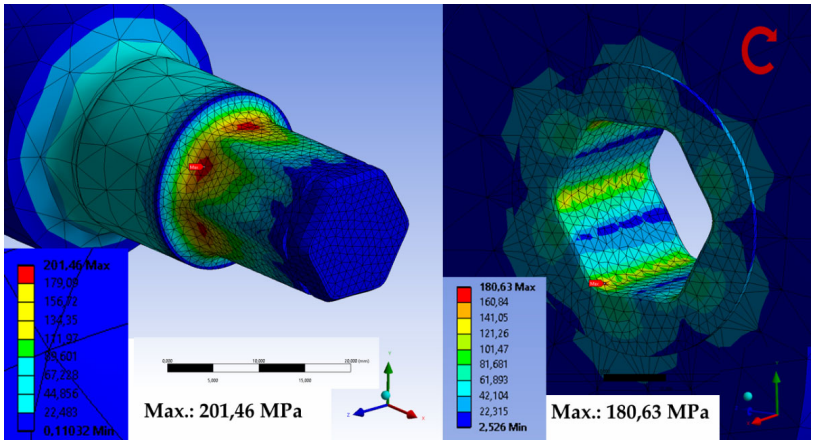

Fundamental for FEM calculations with several bodies is the definition of the contact. For this purpose, the connection type 'frictional' with a coefficient of friction of 0.18 is selected in ANSYS 19 (Ziaei, 2003). The polygon connection of the tests had an H7/n6 fit, which must be considered here. It is a tight transition fit that was modelled using a regressive contact algorithm.

Thereby, the applied standard was the pure penalty algorithm. If there is a penetration of the two bodies, weak springs are generated which make contact and prevent a large penetration. As long as the penetration is small, the results can be considered approximately correct. The penetration is significantly dependent on the load and material properties. To ensure that the penetration remains small, the augmented Lagrange method is used in this calculation. It is a variation of the pure penalty procedure extended by the additional condition that controls the maximum penetration. For this, the contact stiffness of the spring *KN* and the tolerance factor *KL* must be defined as a factor. High values for *KN* and low values for *KL* would be optimal but that would lead to significantly longer calculation times. For both factors, the value 0,1 was used to keep the calculation time and accuracy within limits (Großmann, 2007).

The shaft was fixed at the bearing seats, corresponding to the fixed/floating bearing in the assembled state. For the calculation, a torque of 50 Nm was applied over the outside of the gear. The last shoulder of the output shaft was also rotationally fixed, which means that the shaft, and thus the shaft-hub connection experience the full torque and a static load is present. An example visualisation of a calculation result can be seen in Figure 7.

5.2 Calculation results

As can be seen in the calculation plan, the focus of the calculations was on the H-profile. The aim was to display the equivalent von Mises stresses for the H-profile in three dimensions as a function of the eccentricity and the number of carriers. The results of the equivalent von Mises stresses for the shaft and hub of the H-profiles are shown in Figures 8 and 9. These illustrations clearly show the dependence of the equivalent stresses on the eccentricity and number of carriers. In general, the stresses increase with increasing eccentricity as well as increasing numbers of carriers. In the hub, a continuous increase in equivalent stresses can be observed as a function of eccentricity and the number of carriers. In the shaft, however, the equivalent stresses remain at a constant level up to a number of carriers of approximately 5 and an eccentricity of approximately 0.4 mm. Only with larger values of eccentricity and numbers of carriers is a strong increase in the equivalent stresses noticeable.

Figure 8 H-profiles equivalent von Mises stresses of the shaft (see online version for colours)

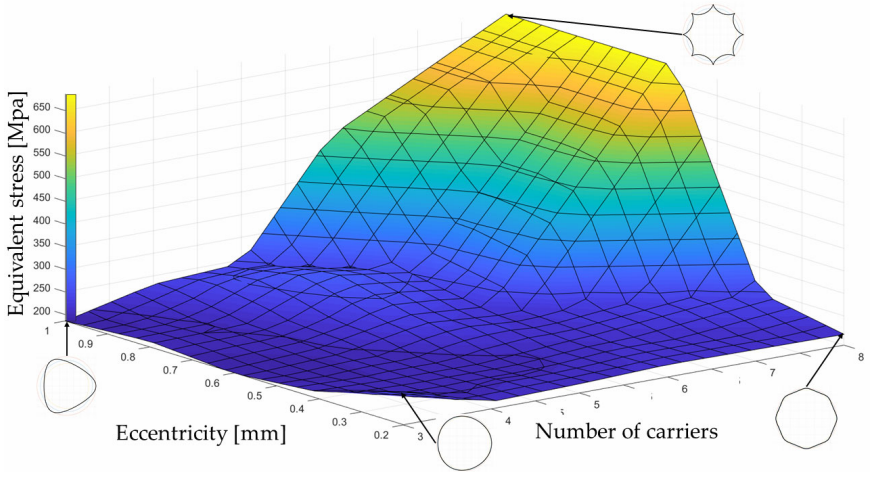

Figures 10 shows the equivalent stresses for different profile types with different eccentricities. All profiles have six carrier elements. Basically, it can also be stated here that the equivalent stresses in the shaft and hub increase with increasing eccentricity. One exception, however, is the H-profile. With this profile, an increase in stresses can only be seen from an eccentricity of 0.4 mm.

The E-profile in Figure 10 shows a strong increase in stress in the shaft depending on the eccentricity. At the same time, the increase in stresses is significantly lower with the E-profile concerning the hub. Comparing the profiles shows that H-profiles are always in the middle range regarding the level of the equivalent stresses. Moreover, the increase in eccentricity only leads to an increase in stresses at larger values than with the other profiles.

The hybrid complex cycloids (M-T04) exhibit significantly high stresses even at very low eccentricities.

Figure 9 H-profiles equivalent von Mises stresses of the hub (see online version for colours)

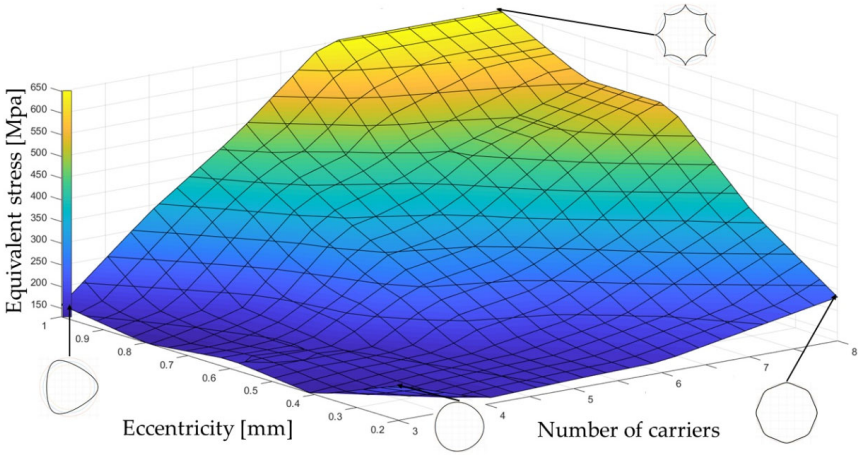

Figure 10 Von Mises equivalent stresses of the shaft and hub of different profiles with six carriers (see online version for colours)

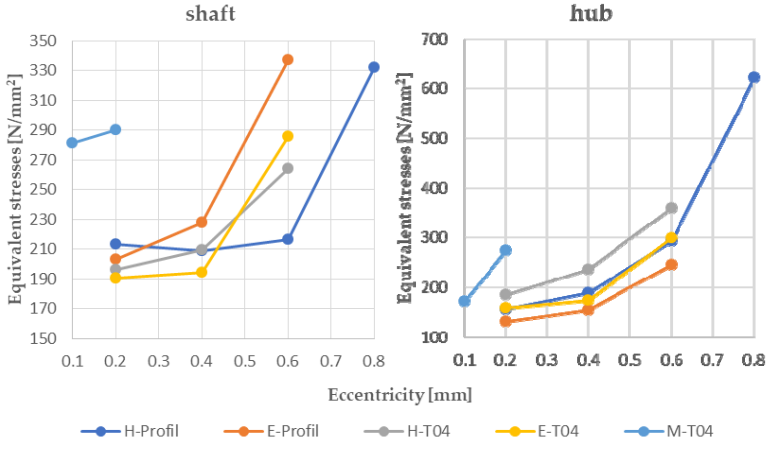

In addition, the behaviour of different profiles with different numbers of carriers was also investigated. For this purpose, the equivalent stresses of the shaft and hub are shown as a function of the numbers of carriers in Figure 11. The eccentricity of the profiles was kept constant in each case. It is 0.6 mm for the H, H-T04, and E-T04 profiles, 0.4 mm for the E-profile, and 0.2 mm for the M-T04 profile. The aim was to achieve better comparability of the profiles, as each profile can be influenced at a different rate by the eccentricity. For example, at an eccentricity of 0.6 mm, the M-T04 profile would already have a contour that is no longer feasible due to overlaps, while the H-profile shows no overlaps at this eccentricity.

Furthermore, it is shown that an increasing number of carriers generally lead to an increase in the equivalent stresses. An exception is the E-profile, where the stresses in the shaft and hub remain constant when the number of carriers is increased. In contrast, the E-T04 profile shows the strongest dependence on the number of carriers in the comparison of the profiles. The H-profile, on the one hand, shows the lowest equivalent

stresses in the shaft even with higher numbers of carriers. On the other hand, the equivalent stresses in the hub are in the upper range for the H-profile. In the H-T04 profile, a larger number of carriers leads to an even greater increase in stresses in the shaft and hub. At low carrier numbers, the complex hybrid profiles show the lowest stresses. However, these stresses increase sharply as the number of carriers increases.

Figure 11 Von Mises equivalent stresses of the shaft of different profiles at constant eccentricities (see online version for colours)

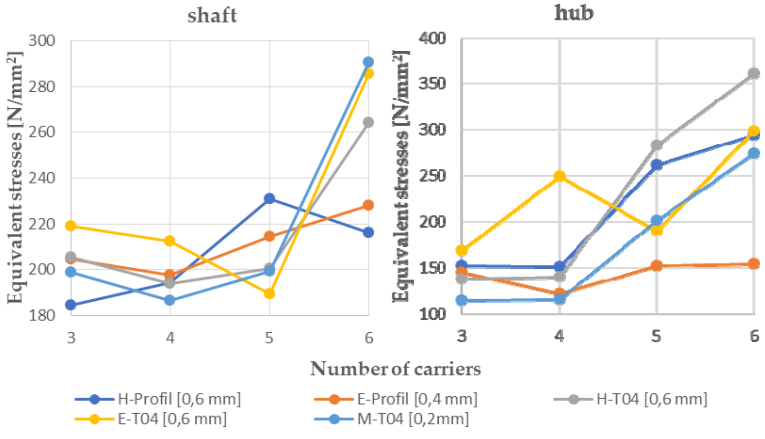

5.3 Discussion of the calculation results

According to the basic geometry, the results of the calculations can be considered plausible. The different graphs of the equivalent stresses of the shaft and hub of the E-profile in Figure 10 can be explained by the geometry. If the eccentricity of the shaft increases, the carrier valleys close more sharply. This results in locally higher peaks of the stresses due to the more pronounced notches. In contrast, flatter and rounder carrier valleys form in the hub, resulting in lower stresses. The complex variant of the E-profile, the E-T04 profile, exhibits significantly lower stresses in the shaft due to the rounded flanks (see Figure 4). The opposite is true for the hub. As described, the H-profiles are in the middle range, whereby they have longer low comparative stresses when the eccentricity in the shaft is increased, as the sharp contours are more likely to occur at the carrier heads. The H-T04 profile tends to have higher stresses in the shaft and hub than the H-profile and is therefore not an improvement.

In the comparative study of the different profiles, it can be summarised that there is no profile that has the lowest stresses in every respect. The E-profiles show a strong eccentricity dependency, at least for the shaft, and form pointed carrier valleys relatively rapid, which limits their use due to high stress levels in the shaft and complicates their manufacturability. This also applies to the hybrid complex profiles, in which the limit of manufacturability is reached even sooner with increasing eccentricity, since undercuts form in the profiles. With respect to the shaft, the E-T04 profiles show improved behaviour in terms of the equivalent stresses as a function of the eccentricity compared to the normal E-profile. If the shaft is assumed to be the weakest component due to its usually smaller cross-section, the H-profile is particularly suitable for a somewhat higher

number of carriers and eccentricities, as the stresses do not increase as much in comparison to the other profiles. The complex variant, the H-T04, does not offer any noticeable improvement in terms of stress levels in the shaft and hub, rather the opposite.

Basically, the level of the equivalent stresses strongly depends on whether it is a shaft or hub. The geometric advantages of a profile for one part of the connection (either shaft or hub) often lead to the opposite effect for its respective counterpart. The H-profile is in the middle range for both the shaft and the hub, which is why this profile is selected for subsequent experimental studies.

The following guidelines for parameter selection for H-profiles can be derived from the calculation results:

- In general, smaller numbers of carriers (between 4 and 6) are recommendable.
- If the number of carriers is small, a larger eccentricity should be selected, since this improves the form fit of the connection and an increase in stresses due to greater eccentricities occurs very late.
- With a higher number of carriers, a lower eccentricity should be selected, because in this case, an increase in the eccentricity quickly leads to an increase in stresses.

According to the FEM calculation results, the optimal H-profile contour has three or four carriers and an eccentricity of 0.6 mm to 0.8 mm. The lowest stresses occur in this range. Nevertheless, an H-profile with an eccentricity of 0.4 mm and six carriers is chosen for the following tests. On the one hand due to manufacturing-related factors and on the other hand to differentiate more from the existing standards, which have three and four carriers, to maximise the gain in knowledge. By choosing multiples of three, self-centring is still possible, and the stresses are distributed over more carriers. The calculations have also shown that the H-profile even with six carriers and an eccentricity of 0.4 mm still yields very low equivalent stresses in both the shaft and the hub.

Figure 12 (a) Recommended H-profile contours and (b) nominal size H6, series 2A according to DIN Deutsches Institut für Normung e.V. (2020) (see online version for colours)

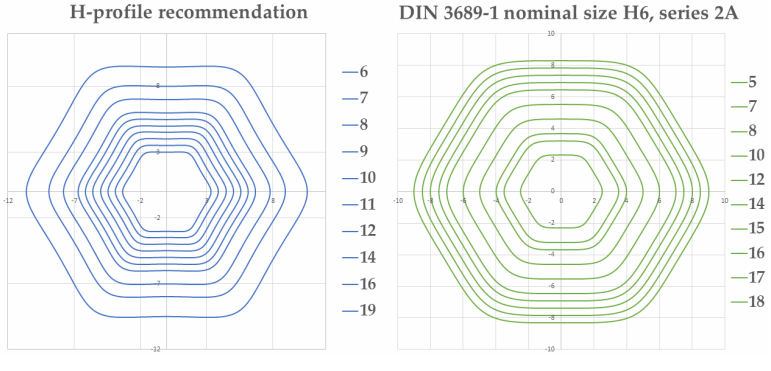

(a) (b)

Since, in theory, the profiles are infinitely scalable, an infinitive number of different diameters can be realised. Figure 12 shows the design guideline we developed with the recommended profile sizes and the associated parameters. The H-profiles all show a geometric similarity to each other, as the relative eccentricity of 0.27 mm is constant for

each of the slightly concave contours. The gradation between the contours is based on the inner diameter d_i of the contour, which in turn is based on the standardised cylindrical shaft diameters of DIN 748-1 (DIN Deutsches Institut für Normung e.V., 1970).

Our recommendations are in line with the DIN 3689-1 specifications (DIN Deutsches Institut für Normung e.V., 2020), which were recently submitted for review and which are also based on the H-profile contours. The DIN profile series is not based on the inner diameter d_i, but on the outer diameter d_a. Nevertheless, the recommendation of this article can be compared with the profile series 2A of nominal size H6. However, the DIN series is based on a slightly lower relative eccentricity of 0.2 mm, resulting in a slightly convex contour, which can have a positive effect on the stresses, as the calculations have shown (DIN Deutsches Institut für Normung e.V., 2020).

6 Experiments

To validate the results of the FEM calculation and to determine the potential of the polygon connection compared to conventional feather key connections, sample parts were manufactured at Nord Drivesystems and static and dynamic long-term experiments were carried out.

6.1 Experiment setups

Comparative dynamic tests up to failure and static tests with polygon and feather key connections in the installed state in the gearbox were carried out. As outlined above an H-profile with six carriers and an eccentricity of 0.4 mm was chosen for the empirical tests.

Figure 13 Endurance test 1 setup (see online version for colours)

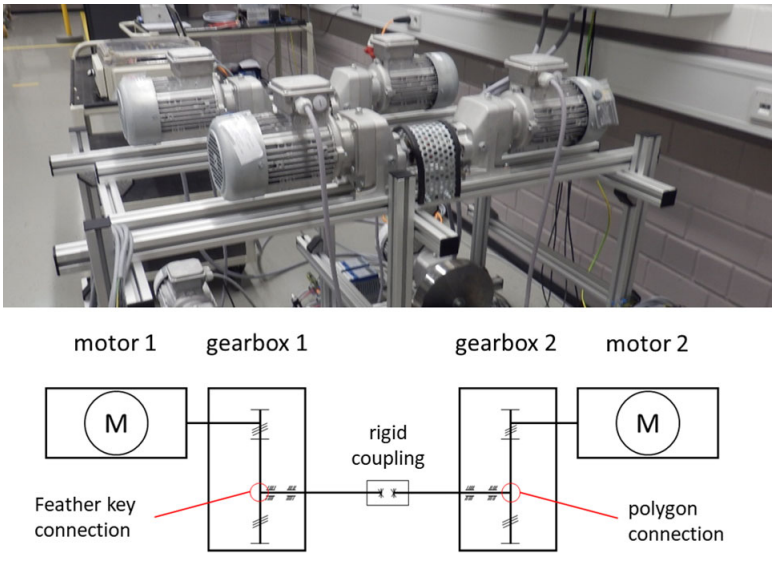

A total of three different long-term tests were carried out by Nord Drivesystems, which essentially differed in their structure and mode of operation. In the first long-term test,

two drive systems, consisting of a motor and a single-stage gearbox, were braced together in accordance with DIN 3952-4 (DIN Deutsches Institut für Normung e.V., 1995), as shown in Figure 13. The aim was to find out which connection would fail first if all boundary conditions were identical. The output shafts of both gearboxes were firmly connected to each other via a rigid coupling. One gearbox was equipped with a feather key connection, the other gearbox with a polygon connection. This experiment was carried out twice.

Figure 14 (a) Long-term test 2 and 3 setup (b) Operating modes (see online version for colours)

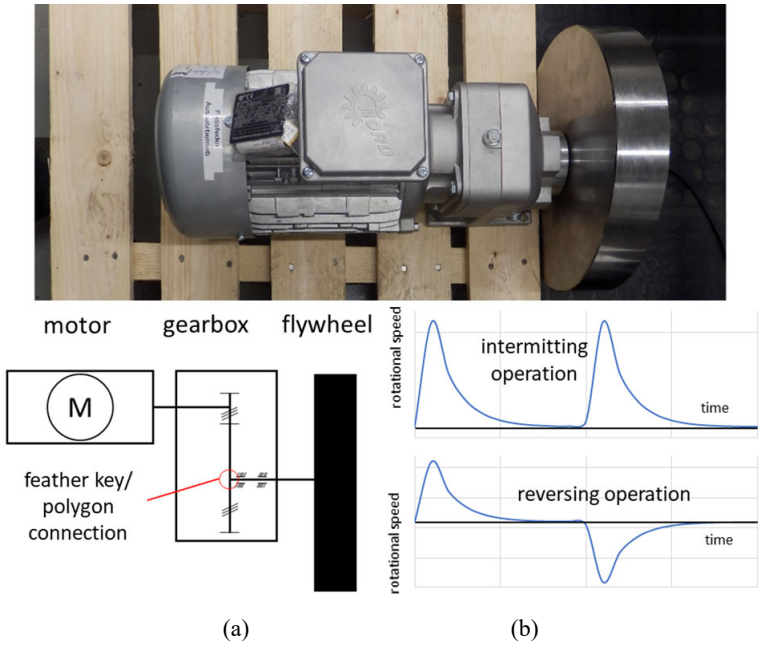

(a) (b)

Figure 15 Static test setup (see online version for colours)

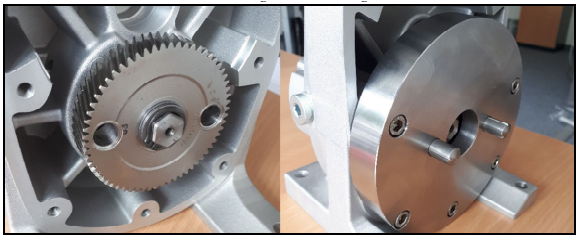

The test setup of the dynamic endurance tests 2 and 3 was identical and only differed in the operating mode. The test setup is shown in Figure 14. The drive unit again consists of a motor and gearbox. A flywheel was mounted on the output shaft. Two gearboxes were used for the test. One gearbox was equipped with a feather key connection and the other one with a polygon connection. Experiment 2 was carried out in intermittent mode, as shown in Figure 14(b). The flywheel was accelerated, run out, and subsequently

accelerated again in the same direction of rotation. Experiment 3 was carried out in reversing mode, whereby after acceleration in one direction the flywheel was then accelerated in the opposite direction. The aim was to record the number of cycles performed until failure. Two gearboxes were again used for the test, one of which was equipped with a feather key connection and the other with a polygon connection.

The aim of the static test was to determine the maximum bearable torque until failure due to fracture. For the test, the shaft was mounted in the housing with the corresponding gear wheel. The static torque was applied evenly manually via a measuring torque wrench on the output side of the shaft. To prevent the torque from resulting in a rotary movement of the shaft with the gear wheel, the rotation had to be blocked. This was achieved by means of two bolts that positively connected the gear wheel and housing form fitting as shown in Figure 15.

6.2 Experimental results

In general, it should be noted that in some tests the load was varied during operation. For example, the load was increased when the runtime became too long, and failure was no longer expected at the current load. This reduces the significance of the test, as greater loads then had to be endured with components that were already pre-stressed. Nevertheless, the increases were always carried out with the polygon and feather key connection at the same time, which means that the tests remain comparable.

Figure 16 Long-term test results (see online version for colours)

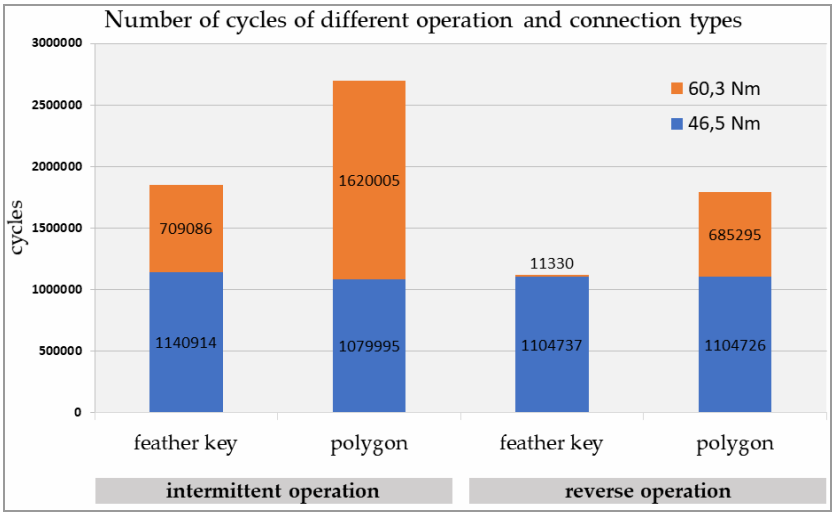

Two tests were carried out during the first long-term test with the gears braced against each other. Here, both trials initially ran for an average of 6,526 hours (272 days) without any gear failure. The load was then increased by running the motors at 4.74 A instead of 3.35 A, which increased the applied torque from 103 Nm to 145 Nm. Subsequently, failures occurred, which in both cases could be attributed to the failure of the feather key connections. The polygon connections in the gearboxes showed no sign of damage or wear.

Figure 16 shows the cycles in comparison to different service life tests in intermittent and reversing operation. In addition, the number of cycles and test torques are shown in detail. In all tests, the load was increased to 60.3 Nm with a similar number of cycles of approx. 1.100.000. Subsequently, failure occurred in all tests, whereby the cycles that run with the higher load differed significantly. If one compares the polygon connection with the feather key connection within an operating mode, for example during intermittent operation, the polygon connection has significantly more cycles (2.700.000) than the feather key connection (1.850.000). Similarly, in reversing operation, the polygon connection has a total of 1.790.000 and the feather key connection 1.116.000 cycles.

Figure 17 shows the fracture surface of the polygon and feather key connection of the long-term test in intermittent operation. The shafts are made from the ductile material C45. Therefore, the material behaviour can best be described with the von Mises hypothesis (maximum-distortion-energy hypothesis). Both fracture surfaces show shearing close to the cross-sectional area. The maximum shear stresses act in this plane during torsion. An edge can be seen on the feather keys, starting from the corner of the keyway, indicating that the crack has formed at this point and has spread from there. In the case of the polygon fracture surface from the experiment, such an edge is not visible.

Figure 17 Fracture surfaces of the long-term tests in intermittent operation, (a) feather key connection (b) polygon connection (sample parts Nord Drivesystems) (see online version for colours)

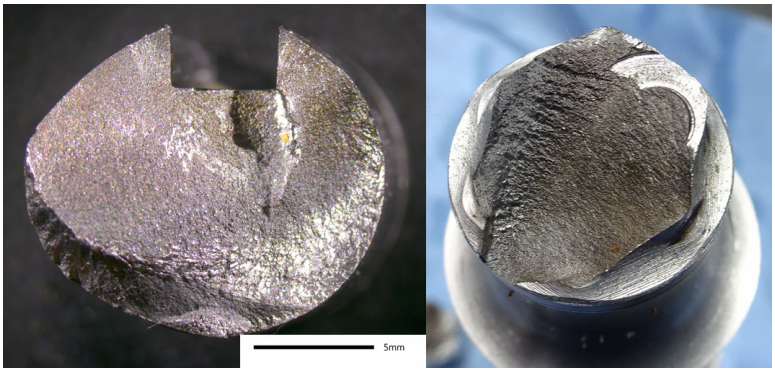

(a) (b)

Figure 18 Fracture surfaces of the long-term tests in reversing operation, (a) feather key connection (b) polygon connection (Nord Drivesystems) (see online version for colours)

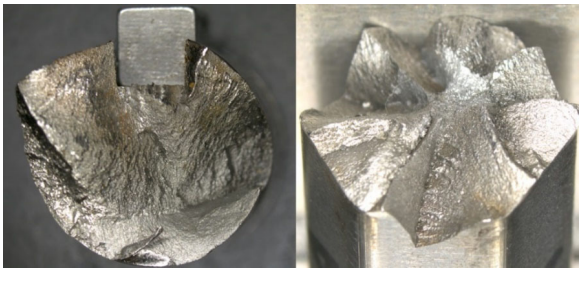

(a) (b)

The fracture surfaces of the tests in reversing mode differ slightly from those in intermittent mode and are shown in Figure 18. The fracture surface of the feather key connection is rougher and has more edges within the fracture surface, indicating a greater proportion of forced fracture. The higher proportion of forced fracture can be explained by the higher dynamic overload in reversing operation. The fracture surface of the polygon connection shows a jagged surface. For comparison, the table of basic forms of oscillatory fractures (Wächter, 1987) was consulted (Figure 19). The fracture surface of the polygon profile corresponds to case 5.4 which is described by a torsional load of a sharp notch at low dynamic overload. The fracture surface of the feather key connection can be assigned analogously to case 5.3 which occurs due to a high dynamic overload. According to the fracture pattern, the feather key connection was subjected to a higher overload than the polygon connection. Since the dynamic load of both connections was identical, it can be inferred that the feather key connection has a lower dynamic load bearing capacity than the polygon connection.

Figure 19 Basic forms of oscillatory fractures (see online version for colours)

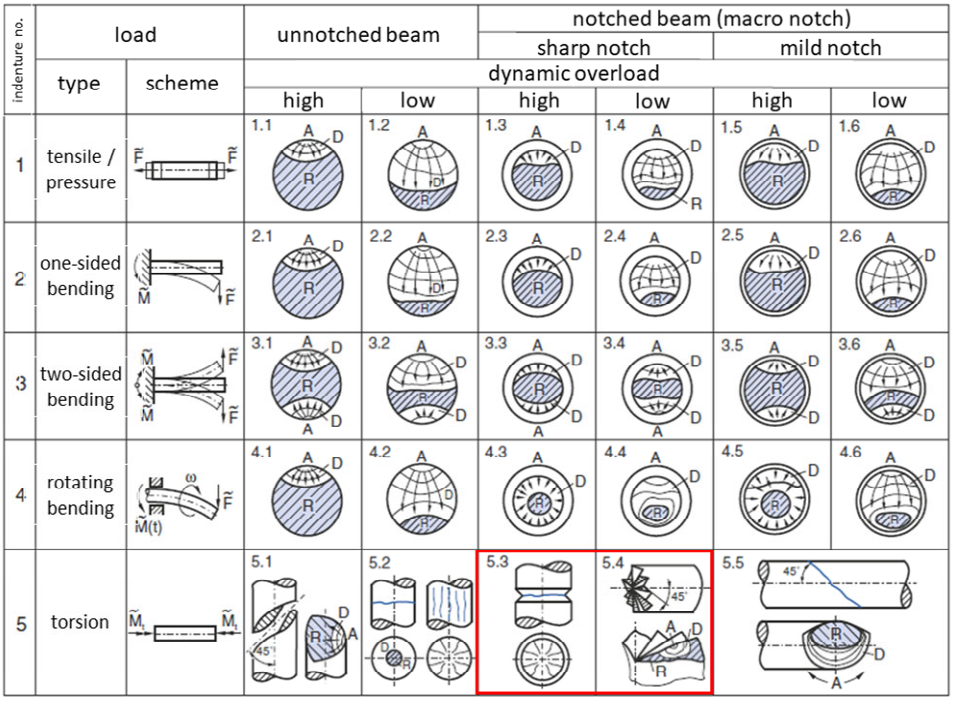

Source: Wächter (1987)

The static test shows that the shaft with polygon connection broke at a torque of 430 Nm. It must be considered that only one test was carried out due to the lack of material and that the measurement inaccuracy of the measuring torque wrench is at least 5 Nm. Therefore, the significance of the experiment is limited but should be sufficient to compare the two connections.

In a direct comparison, the feather key connection was tested statically and failed at a maximum torque of 270 Nm.

6.3 Discussion of the experimental results

The dynamic long-term tests showed that the polygon connections were able to endure a significantly higher cycle number than the feather key connections under the same load. However, it must be considered that the failures were deliberately brought about by increasing the load to shorten the duration of the trials. Since the load was not kept constant during the tests, the fatigue strength of the individual connection cannot be concluded from the tests. As expected, the polygon connection showed a higher dynamic load capacity than the feather key connection.

The static load capacity was also significantly greater within the polygon connection than the feather key connection. Failure occurred within the polygon connection at a torque of 430 Nm while the feather key connection already failed at 270 Nm.

The comparison of the two connections becomes even more expressive when the static load capacity is related to the cross-sectional area or the required installation space. First, the material utilisation is considered by relating the maximum transmittable torque of the connection determined in the tests to the respective cross-sectional area of the shaft. The cross-sectional areas were taken from the CAD system and are A_{Pass} = 139.7 mm^2 for the feather key connection and A_{Poly} = 169.52 mm^2 for the polygon connection. The breaking load related to this cross-sectional area is $2{,}537\frac{Nm}{mm^2}$ for the polygon connection, but only $1{,}933\frac{Nm}{mm^2}$ for the feather key connection. In other words, the polygon connection shows a significantly better material utilisation than the feather key connection, i.e., it can transmit significantly more torque per unit area.

For the comparison of the load bearing capacities in relation to the cross-sectional area, the maximum static moment of the connection determined in the tests is therefore also compared with the collapse load of an equal-area and unnotched circular cross-section (Issler et al., 2003).

The diameter of this circular cross-section can be calculated as follows:

$$d_{kpoly} = 2 * \sqrt{\frac{A_{Poly}}{\pi}} = 14.69\ mm \tag{12}$$

$$d_{kpass} = 2 * \sqrt{\frac{A_{Pass}}{\pi}} = 13.34\ mm \tag{13}$$

This allows the section modulus of torsion to be calculated as follows:

$$W_{T\_kpoly} = \frac{\pi}{16} * \left(d_{kpoly}\right)^3 = 622.69\ mm^3 \tag{14}$$

$$W_{T\_kpass} = \frac{\pi}{16} * \left(d_{kpass}\right)^3 = 466.12\ mm^3 \tag{15}$$

However, the calculated section moduli only apply to stresses in the elastic range. In ductile materials, failure does not occur until the fully plastic state is reached. With the help of the shape factor n_{vpl} = 1.33 of the circular cross-section, the plastic section modulus can be calculated (Issler et al., 2003):

$$W_{Tvpl\_kpoly} = n_{vpl} * W_{T\_kpoly} = 828.18\ mm^3 \tag{16}$$

$$W_{Tvpl\_kpass} = n_{vpl} * W_{Tkpass} = 619.94\ mm^3 \tag{17}$$

For the calculation of the maximum stresses that can be borne in the fully plastic state, the collapse characteristic value $\overline{R}$ can be used as a good approximation, which represents the arithmetic mean of the yield strength and maximum tensile strength (Issler et al., 2003). For the calculation of $\overline{R}$, a yield strength of R_{eTB} = 490 *MPa* and a tensile strength of R_{mTB} = 700 *MPa* (DIN Deutsches Institut für Normung e.V., 2012) are needed. Since the test shaft has a larger diameter than 16 mm, the technological size influence factor $K_1(d_{eff})$ according to DIN 743 (DIN Deutsches Institut für Normung e.V., 2012) must be taken into account:

$$R_e = \left(1 - 0.34 * \lg\left(\frac{d_{eff}}{d_B}\right)\right) * R_{eTB} = 433.36 \frac{N}{mm^2} \tag{18}$$

$$R_m = \left(1 - 0.26 * \lg\left(\frac{d_{eff}}{d_B}\right)\right) * R_{mTB} = 638.13 \frac{N}{mm^2} \tag{19}$$

According to DIN 743 (DIN Deutsches Institut für Normung e.V., 2012), the reference diameter d_B = 16 mm must be used. The diameter d_{eff} depends on the shaft geometry and in this case, is 35 mm. The value $\overline{R}$ is calculated as follows:

$$\overline{R} = \frac{R_e + R_m}{2} = 535.75 \frac{N}{mm^2} \tag{20}$$

With (16) or (17) and (20), the collapse loads, i.e., the maximum torque that can be carried by the two comparison cross-sections, can be calculated:

$$M_{Tvpl\_kpoly} = \overline{R} * W_{Tvpl_{kpoly}} = 443.7 Nm \tag{21}$$

$$M_{Tvpl\_kpass} = \overline{R} * W_{Tvpl_{kpass}} = 332.13 Nm \tag{22}$$

From this, it follows that the maximum static torque that can be carried is approximately 3% smaller for a polygon connection, but approx. 19% smaller for the feather key connection than for an unnotched circular cross-section with an equal sectional area.

In practice, it is relevant how much torque can be transmitted in a defined installation space. For this purpose, the maximum static moment determined in the tests is compared with the collapse load of an unnotched circular cross-section that has the same installation space as the polygon connection respectively the feather key connection. The diameter serves as a parameter for the installation space, via which the collapse load can be calculated using the plastic section modulus. In the case of the feather key connection, the cross-section equal to the installation space is A_{Pass_b} = 153.93 mm^2, in the case of the polygon connection A_{Poly_b} = 172.03 mm^2. The calculation procedure of the collapse load for the circular cross-section equal to the building space is identical to the calculation already presented in equations (12) to (22). This results in a collapse load of 383.91 Nm for the feather key connection and 453.55 Nm for the polygon connection. The maximum tolerable torque is therefore approx. 30% lower with the feather key connection, but only 5% lower with the polygon connection compared to an un-notched circular cross-section

with the same installation space. The larger discrepancy between the polygon connection and the feather key connection in this comparison can be attributed to the deep notch of the feather key connection which significantly weakens the cross-section compared to an un-notched circular cross section of the same installation space.

All results presented in this section are listed in Table 3 for a better overview. It can be seen that the feather key connection causes a significantly greater weakening of the cross-section than the polygon connection.

Table 3 Comparison values for feather key and polygon connection

	Feather key connection	*Polygon connection*	*Unit*
Test collapse load	270	430	Nm
Cross-sectional area	139.7	169.52	mm^2
Cross-sectional breaking load in the test	1,933	2,537	Nm/mm^2
Weakening compared to circular cross-section with equal cross-sectional area	19	3	%
Weakening compared to a circular cross-section with equal installation space	30	5	%

In summary, the comparison shows that the polygon connection is superior to a comparable feather key connection regarding the static load bearing capacity. The fact that the feather key connection has sharp corners where stress peaks form causes the breakage to occur much sooner. With the polygon connection, in contrast, the torsional moment can be transmitted more evenly over six carriers and the local stress peaks therefore lowered.

7 Conclusions and outlook

The aim of this work was to illustrate the stress behaviour of polygon profiles as a function of the number of carriers and eccentricity and to derive dimensioning and design guidelines with concrete contour recommendations. In addition, the advantages of the polygon connection compared to feather key connections were demonstrated. For this purpose, both extensive FEM calculations and practical tests were carried out.

The FEM calculations showed a general increase in equivalent stresses with increasing numbers of carriers and increasing eccentricity. The H-contour turned out to be the most suitable profile in a direct comparison with the other profile types, as the comparative stresses were relatively low both in the shaft and the hub. Regarding the associated parameters, the following design guidelines can be defined:

- a reduced number of carriers (four to six carriers) should be chosen
- lower eccentricity should be selected for larger numbers of carriers
- higher eccentricity is recommended with fewer carriers.

The optimum profile identified in this work was the H-profile with six carriers and an eccentricity of 0.4 mm, which comes closest to the nominal size H6 of series 2A of the forthcoming DIN 3689-1 (DIN Deutsches Institut für Normung e.V., 2020).

Subsequently, the H-profile was directly compared with a feather key connection by means of tests. With the help of the static load test, the maximum bearable torque was determined for both shaft-hub connections. This was 270 Nm for the feather key connection and 430 Nm for the polygon connection. Compared with an un-notched circular cross-section with the same cross-sectional area, the breaking loads of the feather key connection and the polygon connection were 19% and 3% lower, respectively. Compared with an un-notched circular cross-section with the same installation space, the breaking loads of the feather key connection and the polygon connection were 30% and 5% lower, respectively.

The polygon connection also exhibited a better dynamic load bearing capacity in the dynamic long-term tests. In the comparative tests in which feather key and polygon connections were cyclically loaded in intermittent and reversing operation, the polygon connection achieved higher cycle numbers. As expected, the polygon connection was superior to the feather key connection with respect to both static and dynamic load bearing capacity.

For the widespread use of the new polygon profiles in industry, an analytical proof of strength must first be developed for them – analogous to other machine elements. Such an analytical strength verification will be part of DIN 3689 part 2, which is yet to be published. Furthermore, production possibilities must be examined individually for each company, as the production of polygon profiles requires modern turning or milling centres. These aspects will eventually be covered in part 3 of DIN 3689.

Acknowledgements

The authors thank the Department of Mechanical Engineering and Production Management and the Faculty of Engineering and Computer Science of the Hamburg University of Applied Sciences (HAW Hamburg) for funding the Open Access publication fee. The authors also thank Nord Drivesystems for their support in carrying out the empirical tests.

References

DIN Deutsches Institut für Normung e.V. (1970) *Zylindrische Wellenenden; Abmessungen, Nenndrehmomente*, DIN 748-1. Beuth Verlag, Berlin.

DIN Deutsches Institut für Normung e.V. (1995) *Vereinfachte Darstellung in der Kinematik. Teil 4: Verschiedene Getriebe und deren Zubehörteile*, DIN 3952-4. Beuth Verlag, Berlin.

DIN Deutsches Institut für Normung e.V. (2009a) *Welle-Nabe-Verbindung – Polygonprofil P3G*, DIN 32711. Beuth Verlag, Berlin.

DIN Deutsches Institut für Normung e.V. (2009b) *Welle-Nabe-Verbindung – Polygonprofil P4C*, DIN 32712. Beuth Verlag, Berlin.

DIN Deutsches Institut für Normung e.V. (2012) *Tragfähigkeitsberechnung von Wellen und Achsen*, DIN 743. Beuth Verlag, Berlin.

DIN Deutsches Institut für Normung e.V. (2020) *Welle-Nabe-Verbindung – Hypotrochoidische H-Profile. Teil 1: Geometrie und Abmessungen*, DIN 3689-1, Beuth Verlag, Berlin.

Erven, J. and Schwägerl, D. (2011) *Mathematik für Ingenieure*, 4th ed., Oldenbourg Wissenschaftsverlag GmbH, München.

Frank, A. and Pflanzl, M. (1998) 'Die Norm-Polygonverbindungen P3G und P4C. Geometrische Grundlagen, Funktionsverhalten und Fertigung', in Verein Deutscher Ingenieure (Ed.): *Welle-Nabe-Verbindungen. Systemkomponenten im Wandel*, VDI – Berichte 1790, VDI Verlag GmbH, Düsseldorf, pp.105–120.

Frank, A., Trantin, H. and Pflanzl, M. (2003) 'Die 'Polygon – Normen' DIN 32711 und DIN 32712 – 'Upgrading' oder Neunormung', in Verein Deutscher Ingenieure (Ed.): *Welle-Nabe-Verbindungen. Gestaltung, Fertigung, Anwendung*, VDI – Berichte 1384, VDI Verlag GmbH, Düsseldorf, pp.77–89.

Großmann, C. (2007) *Fretting Fatigue of Shape Optimised Polygon-Shaft-Hub Connections*, Berlin.

Issler, L., Ruoß, H. and Häfele, P. (2003) *Festigkeitslehre – Grundlagen*, 2nd ed., Springer-Verlag, Berlin.

Leidich, E., Schreiter, R. and Knorr, P. (2016) 'Belastbarkeit von H-Profil-Welle-Nabe-Verbindungen', *Antriebstechnik*, No. 8, pp.76–81.

Selzer, M. and Ziaei, M. (2016) 'Zykloiden höherer Stufe – Alternative für formschlüssige Welle-Nabe-Verbindungen Teil 1', *Antriebstechnik*, No. 10, pp.100–105.

Vetter, S., Leidich, E. and Hasse, A. (2020) 'Gestaltfestigkeit von hypotrochoiden Polygon-Welle-Nabe-Verbindungen/Fatigue strength of hypotrochoidal polygon-shaft-hub connections', *Konstruktion*, Vol. 72, Nos. 05–06, pp.76–82, https://doi.org/10.37544/0720-5953-2020-05-06-76.

Wächter, K. (1987) *Konstruktionslehre für Maschineningenieure Grundlagen*, *Konstruktions-und Antriebselemente*, 1st ed., VEB Verlag Technik, Berlin.

Ziaei, M. (2003) *Analytische Untersuchung unrunder Profilfamilien und numerische Optimierung genormter Polygonprofile für Welle-Nabe-Verbindungen*, Chemnitz.

Ziaei, M. (2007a) 'Anpassungsfähige kontinuierliche Innen-und Außenkonturen für form-und reibschlüssige Verbindungen auf Basis der komplexen Zykloiden', in VDI Wissensforum IWB GmbH (Ed.): *Welle-Nabe-Verbindungen*, DI – Berichte 2004, VDI Verlag GmbH, Düsseldorf, pp.277–294.

Ziaei, M. (2007b) 'Neue Berechnungskonzepte zur Dimensionierung von standardisierten Polygonprofilen für formschlüssige Welle-Nabe-Verbindungen', in VDI Wissensforum IWB GmbH, (Ed.): *Welle-Nabe-Verbindungen*, VDI – Berichte 2004, VDI Verlag GmbH, Düsseldorf, pp.41–55.

Ziaei, M. (2012) 'Optimale Welle-Nabe-Verbindung mit mehrfachzyklischen Profilen. Vergleichende Untersuchung an komplexen Trochoiden', in *Welle-Nabe-Verbindungen*, VDI Wissensforum IWB GmbH (Ed.) VDI – Berichte 2176, VDI Verlag GmbH, Düsseldorf, pp.233–245.

Nomenclature

A_{Pass}	Cross-sectional area feather key connection
A_{Poly}	Cross-sectional area polygon connection
d	Diameter
d_a	Outer diameter
d_B	Reference diameter
d_{eff}	Effective diameter
d_i	Inner diameter

d_{kpass}	Circular cross-section diameter comparable to the shaft with the feather key
d_{kpoly}	Circular cross-section diameter comparable to the shaft with the polygon profile
e	Eccentricity
e_0	Base eccentricity
f_{xn}, f_{yn}	Function of eccentricities
K_B	Base circle
K_R	Rolling circle
$K_1(d_{eff})$	Technological size influence factor
M	Centre of the rolling circle
MT_{vpl_kpass}	Maximum torque (feather key)
MT_{vpl_kpoly}	Maximum torque (polygon)
n	Periodicity (corner number)
n_{vpl}	Shape factor for a circular cross-section
P	Contour generating point
R_e	Yield strength
R_{eTB}	Yield strength (table value)
R_m	Tensile strength
R_{mTB}	Tensile strength (table value)
$\overline{R}$	Collapse characteristic value
r	Nominal radius
t	Parameter angle
W_{T_kpass}	Section modulus of torsion for a circular cross-section related to the feather key shaft
W_{T_kpoly}	Section modulus of torsion for a circular cross-section related to the polygon shaft
W_{Tvpl_kpass}	Plastic section modulus of torsion for a circular cross-section related to the feather key shaft
W_{Tvpl_kpoly}	Plastic section modulus of torsion for a circular cross-section related to the polygon shaft
α_n	Function of the main parameter angle t
ε	Relative eccentricity

Abbreviations

CAD	Computer-aided design
DIN	Deutsches Institut für Normung e.V. (German Institute for Standardisation e.V.)
E	Epitrochoid
E-T04 (ET)	Pure complex epitrochoid with four eccentricities
FEM	Finite element method
H	Hypotrochoid
H-T04 (HT)	Pure complex hypotrochoid with fours eccentricities
KL	Tolerance factor
KN	Contact stiffness of the spring
M-T04 (MT)	Hybrid complex trochoid with four eccentricities
P3G	Defined geometry by DIN 32711
P4C	Defined geometry by DIN 32712